DETECTION OF THE DEFORMATION RATE GAPS BETWEEN BUILDINGS AND LAND SURFACE BY DIFFERENTIAL SYNTHETIC APERTURE RADAR INTERFEROMETRY TECHNIQUES

Naoyuki Maruo[1], Junichi Susaki[1], Tirawat Boonyatee[2], Kiyoshi Kishida[1]
[1] Graduate School of Engineering, Kyoto University,
C1-1-209, Kyotodaigakukatsura, Nishikyo-ku, Kyoto, 615-8540, Japan
Email: {maruo.naoyuki.36x, susaki.junichi.3r, kishida.kiyoshi.3r}@kyoto-u.ac.jp
[2] Department of Civil Engineering, Faculty of Engineering,
Chulalongkorn University, Phayathai, Bangkok, 10330, Thailand
Email: dr.tirawat@gmail.com

KEY WORDS: land subsidence, slip-up, Differential interferometric synthetic aperture radar (DInSAR), Persistent Scatterer Interferometry (PSI), Small Baseline Subset (SBAS)

ABSTRACT: This paper presents a differential interferometric synthetic aperture radar (DInSAR) combination approach to detect slip-up phenomena, gaps between building bases and land surface. We assume that the information about building surface displacement can be extracted from single look SAR images whereas the information about land surface deformation can be extracted from multi look SAR images. The proposed method implements Persistent Scatterer Interferometry (PSI) and Small Baseline Subset (SBAS) techniques for respective purposes. Subtraction of the two results can detect the phenomena. In addition, the proposed method improved the PSCs selection introducing phase analysis. The comparison with the annual leveling data has demonstrated the reliability of SBAS result for the estimation of land surface estimation, and the comparison with the field survey data has demonstrated the possibility of our approach to apply for the detection of slip-up occurring area, respectively.

1. INTRODUCTION

Land subsidence from excessive amount of ground water extraction has occurred in many urban cities all over the world which have been rapidly developing in a last few decades. It has caused a lot of negative impacts to those cities, for example, increasing risk of flooding in coastal areas, cracking the buildings and infrastructures, destructing local groundwater systems, and generating tension cracks on land and reactivating faults. Among the negative impacts of land subsidence in the urban cities, we especially focus on slip-up phenomena of the buildings in this paper. Figure 1 shows an example of the slip-up phenomena in our study area, Bangkok, Thailand. The buildings using pile foundation are supported by the less compressible load bearing layer and show less or no subsidence compared to the surrounding land surface which sinks due to the land subsidence. As a result, buildings are as if slipping up from the viewpoint of the land surface, which we call as slip-up phenomena. The phenomena may break buried pipes connecting to the buildings, cause the floor instability, or encourage insects to live in the cavity caused by it. Therefore, it is important to inspect regularly the condition of the buildings in the area where this kind of slip-up is occurring.

In our preliminary study, we found that different characteristic of the phase information can be extracted from single look pixels, and multi look pixels, and that they are partly consistent with displacement rates of the scatterers (such as the buildings) and the land surface, respectively. Typically, persistent scatterers are parts of artificial structures such as bridges, facades or building corners. Therefore, if a persistent scatterer is from a building, the result of displacement analysis of the pixel may reflect the building displacement. On the other hand, multi look pixel signal consists of the sum of random signals and the result of displacement analysis of the multi look pixel is likely to reflect larger scale displacement such as the land surface displacement. Therefore, in this paper, we propose a method to extract displacement information via single look and multi look differential interferometric synthetic aperture radar (DInSAR) analysis, Persistent Scatterer Interferometry (PSI) (Ferretti et al., 2000) and Small Baseline Subset (SBAS) (Berardino et al., 2002). PSI can provide time series deformation of individual persistent scatterers such as buildings whereas SBAS can provide spatially large scale deformation (land surface deformation). This paper is organized as follows. The study area and data used are presented in Section 2. The proposed method to detect slip-up phenomena is then presented in Section 3. The results are shown and discussed in Sections 4 and 5, respectively. Finally, Section 6 concludes this paper.

2. STUDY AREA AND DATA USED

We selected Bangkok, capital of Thailand as a study area. It is reported that Bangkok has been suffering from the gaps

Figure 1. Slip-up phenomena observed in Bangkok. The red arrow shows the slip-up, a gap between the building base and ground.

caused by different displacement rates between building and land surfaces. Bangkok has a compressible soft cray of the 12-16 m thick layer at the ground surface. The first sand layer (Upper Bangkok aquifer) is underlying the soft clay layer and the first stiff clay layer is mostly at 22-24 m depth below the ground surface in the inner city area [4]. Since the compression of these shallow clay layers is a large portion of the total subsidence observed at the ground surface, most of the buildings rest on piles standing on less compressible sand layer 20-50 m below the surface. As a result, slip-up phenomena have been reported in Ladkrabang district, Eastern Bangkok, and other parts of the city as well (Anuphao, 2012).

In this research, we used 14 Advanced Land Observing Satellite (ALOS)/Phased Array type L-band SAR (PALSAR) level 1.1 (L1.1) data acquired from November 2007 to December 2010 on the ascending orbit. The resolution of a SAR image is about 3.1 m in the azimuth and 7.5 m in the range direction, respectively. We also used the SRTM3 DEM with a nominal resolution of 90 × 90 m to remove phase fringes induced by the topography. The area of the scene is shown in Fig. 2. For the validation of the land surface deformation results, we used 15 of 1 m-depth-leveling data measured by Royal Thai Survey Department (RTSD) in annual leveling survey. The measurements are the first-order leveling survey and the accuracy is in centimeter level (Royal Thai Survey Department, 2003). For the validation of detection result of slip-up phenomena, we conducted field survey in districts, shown in Figure 2 (b). Hereafter, we refer these districts as Area A. Area A is a part of Ladkrabang district where slip-up phenomena have been reported and actually measured by our field survey. We measured vertical gaps at 18 sites in Area A.

3. METHOD

In this section, we describe the proposed method to estimate land surface displacement in Bangkok as well as the detection of slip-up occurring area. We divide the section into three parts, PSI processing part, SBAS processing part, and combination part of the both estimated deformation results. In the first two parts, we basically follow the general concepts and outlines of the conventional methods introduced by Ferretti et al. (2000) and Berardino et al. (2002) for PSI and SBAS, respectively. Here, we emphasize the difference of our method from the referential methods and explain actual used values such as selected interferometric pairs or threshold to the study area in our approach. Finally, combination process of the results by the two methods is described.

3.1 PSI processing

We selected January 2009 data as a master image based on the dispersion of the perpendicular baselines (Colesanti et al., 2003), and generated 13 interferograms with respect to master images. We implemented the process to Area A. The processed area is limited to approximately 8 km by 8 km to reduce the computational effort and propagation error of parameters estimation. The size of the area is adequate enough for our purpose to make use of SAR data as screening of slip-up occurring area.

For the PSCs selection, we conducted not only amplitude analysis but also phase analysis. In the amplitude analysis step, we used a relatively loose value of 0.3 as a threshold of the amplitude dispersion index, which leads to most of the selected pixels not being PS pixels. This process is for reducing the initial number of pixels for next step, phase analysis, which we refer as Selective PSCs (SPSc) selection.

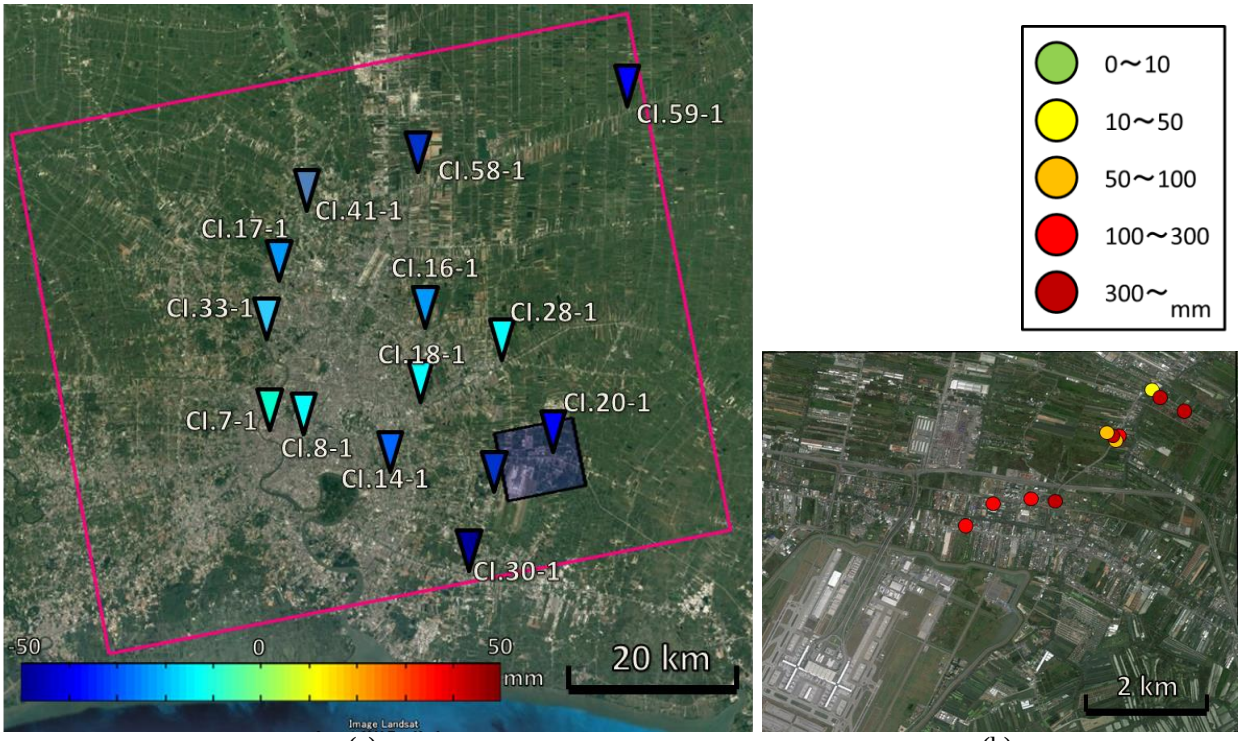

(a) (b)

Figure 2. Study area in the present research. (a) Google Earth image around Bangkok, Thailand. The pink rectangle corresponds to the area of ALOS/PALSAR images, and the names of the inverted triangles are the ones for leveling. (b) Area A around Suvarnabhumi Airport, shown by a blue rectangle in (a). The colors of the points where field survey was conducted have denote slip-up values.

3.1.1 SPSCs selection: We start with the description of differential interferogram phase calculation. After the removal of the topographic phase using external DEM, the phase, $\varphi_{x,i}$, of the xth pixel in the ith unwrapped differential interferometric phase, is expressed as follows:

$$\varphi_{x,i} = \varphi_{h,x,i} + \varphi_{d,x,i} + \varphi_{a,x,i} + \varphi_{o,x,i} + \varphi_{n,x,i} \quad (1)$$

where $\varphi_{h,x,i}$ is the phase due to inaccuracy of external DEM, $\varphi_{d,x,i}$ is the phase due to the displacement of the scatterer, $\varphi_{a,x,i}$ is the phase due to atmospheric delay, $\varphi_{o,x,i}$ is the phase due to an orbital error, and $\varphi_{n,x,i}$ is decorrelation noise.

In Equation (1), the contribution of the first four terms dominates the noise term, making it difficult to identify the low phase standard deviation pixels. Therefore, in order to obtain an estimates for the noise term, $\varphi_{n,x,i}$, these four terms should be estimated and removed from the interferometric phase, $\varphi_{x,i}$. The first four term in Equation (1) are spatially correlated except for the DEM error, $\varphi_{h,x,i}$, which tends to be partly spatially correlated. To estimate the spatially correlated component of the phase, Hooper et al., 2007 proposed to apply a band-pass filter that adapts to any phase gradient present in the data. They implemented a band-pass filter as an adaptive phase filter combined with a low-pass filter, applied in the frequency domain.

Firstly, each pixel is weighted by setting the amplitude in all interferograms to an estimate of the SNR for the pixel, which in the first iteration it is set as $1/D_{\mathcal{A}}$. Secondly, the complex phase of the weighted pixels is sampled to a grid with spacing of 200 m to enable using 2-D fast Fourier transform. Thirdly, 2-D FFT is applied to a grid size of 32-by-32 cells and the intensity is smoothed by convolution with a 7-by-7 pixel Gaussian window Equation (2). Fourthly, the adaptive phase filter response, $H(u,v)$, is combined with a narrow low-pass filter response, $L(u,v)$, to form the new filter response, $\mathrm{G}(u,v)$ Equation (3), and by applying the new filter to the resampled observed phase in frequency domain, $FFT[\varphi_{x,i}]$, the spatially correlated phase component, $\tilde{\varphi}_{x,i}$, will be obtained after 2-D inverse FFT Equation (4).

$$H(u,v) = \left|Gaussian(u,v) * FFT\left[\varphi_{x,i}\right]\right| \tag{2}$$

$$G(u,v) = L(u,v) + 0.3\left(\frac{H(u,v)}{\bar{H}(u,v)} - 1\right) \tag{3}$$

$$\tilde{\varphi}_{x,i} = IFFT\left[G(u,v) * FFT\left[\varphi_{x,i}\right]\right] \tag{4}$$

where $L(u,v)$ is the fifth-order Butterworth filter, with a typical cutoff wavelength of 800 m, and $\bar{H}(u,v)$ *i*s the median value of $H(u,v)$.

Fifthly, subtracting the filtered phase, $\tilde{\varphi}_{x,i}$, from the observed phase, $\varphi_{x,i}$, and rewrapping. This will give an estimation of the spatially uncorrelated phase Equation (5). The second term in the right hand side of Equation (5) is expected to be small, therefore we will replace this term by δ. As for the first term, the effect DEM error, $\varphi_{h,x,i}$ can be estimated using a periodogram Equation (6), where, $B_{\perp}$ is the perpendicular baseline, λ is the signal wavelength, h_x is the DEM error height, R_x is the sensor target distance and ϑ_x is the incident angle.

$$W\{\varphi_{x,i} - \tilde{\varphi}_{x,i}\} = W\{\varphi^u_{h,x,i} + \varphi^u_{d,x,i} + \varphi^u_{o,x,i} + \varphi^u_{a,x,i}\} + W\{\varphi^u_{h,x,i} + \phi_{Noise}\} \tag{5}$$

$$argmax_h\left\{\gamma_x(h_x) = \frac{1}{N}\left|\sum_{i=1}^{N}\left\{expj\left(\varphi_{x,i} - \tilde{\varphi}_{x,i} - \frac{4\pi}{\lambda}\frac{B_{\perp,i}}{R_x \cdot sin(\vartheta_x)} \cdot h_x\right)\right\}\right|\right\} \tag{6}$$

Sixthly, subtracting the estimated phase due to DEM error, $\hat{\varphi}^u_{h,x,i}$, from Equation (6), and assuming that $\delta \approx 0$, makes Equation (7) to be the first estimation of the noise component $\hat{\phi}_{Noise}$.

$$W\{\Phi_{InSAR} - \tilde{\varphi}_{x,i} - \hat{\phi}^{Res}_{Topo}\} = W\{\delta + \hat{\phi}_{Noise}\} \tag{7}$$

Seventhly, using the estimated noise phase $\hat{\phi}_{Noise}$ to calculate the SNR for every pixel using Equation (6), where g is the signal amplitude which assumed to be constant, A is the observed amplitude and $\hat{\sigma}_n^2$ is the noise variance. Finally, to get a better estimate for the noise phase, the process should be repeated using the estimated SNR as a weight factor. The system converges when the difference of γ_x between iterations cease of decreasing. In this analysis, we selected SPSCs by setting a threshold value of 0.9 to the final estimation of γ_x.

3.1.2 Orbital error removal: In the general PSI processing, orbital error term, $\varphi_{o,x,i}$ and atmospheric delay term, $\varphi_{a,x,i}$, are treated in one hand since both effects are similar between neighboring pixels and can be regarded as the residual phase when we difference $\varphi_{x,i}$ between neighboring SPSCs pixels along all the arcs of SPSCs network. However, in ALOS PALSAR case, due to the less precise orbital information, the gradient of the interferometric phase ramp in each interferogram is relatively large and may affect the deformation parameters estimation. Therefore, we applied orbital phase error correction to the wrapped interferograms to avoid phase unwrapping error. The orbital phase error term is assumed as a linear plane. To estimate linear phase ramp parameters b_i and c_i of ith interferogram without phase unwrapping, we used a simple periodogram as

$$argmax_{b,c}\left\{\gamma(\hat{b},\hat{c}) = \frac{1}{M}\left|\sum_{x=1}^{M}\left\{expj\left(\Delta\varphi_{x,i} - (b_i \cdot \xi_x + c_i \cdot \eta_x)\right)\right\}\right|\right\} \tag{8}$$

where M is the number of SPSCs pixels, ξ_x and η_x are the range and the azimuth coordinates at the points, and γ is an indicator of how well the linear plane model is fit to the interferogram.

After orbital error removal, we estimated parameters on the arcs using refined interferograms and integrated the

estimated parameters along the arcs, generating the linear displacement velocity and DEM error height at remained SPSCs pixels, which we finally regarded as PSs.

3.1.3 PS density increment step: In this step, we estimate the parameters on the PSCs points which are rejected to be as SPSCs in the phase analysis step. Connecting with 4 neighboring SPSCs, phase differences are calculated and the parameters on the arcs are estimated on all the connected arcs, obtaining temporal coherence vector, $\hat{\boldsymbol{\gamma}}$, linear displacement velocity difference vector, $\Delta\hat{\boldsymbol{v}}$, and DEM error height difference vector, $\Delta\hat{\boldsymbol{h}}$. If mean of coherence vector is larger than 0.9, we add the PSC as PS points and estimate the parameters as

$$\hat{v}_{PSC} = \frac{1}{\sum_{i=1}^{4} \hat{\gamma}_{t,i}} \sum_{i=1}^{4} \{\hat{\gamma}_{t,i}(\hat{v}_i + \Delta\hat{v}_i)\} \tag{9}$$

$$\hat{h}_{PSC} = \frac{1}{\sum_{i=1}^{4} \hat{\gamma}_{t,i}} \sum_{i=1}^{4} \{\hat{\gamma}_{t,i}(\hat{h}_i + \Delta\hat{h}_i)\} \tag{10}$$

We calculate this step for all the left PSCs. As for the filtering step to estimate nonlinear deformation terms from the residual phase, we used 200 m by 200 m 2-d Gaussian filter in space and 365 days 1-d Gaussian filter in time domain.

3.2 SBAS processing

First of all, the 16-look and 32-look multilookings were applied to interferogarms in the range and azimuth directions, respectively; hence, the pixel spacing was approximately 100× 100 m in both directions. Among total of 14 SAR images, we generated 26 interfefrograms such that a perpendicular baseline value is smaller than 1,000 m and the mean value of the coherence of an interferograms exceeds 0.2. As for phase unwrapping process, we used Minimum Cost Flow, setting the unwrapping coherence threshold value of 0.2. After phase unwrapping, we corrected orbital error phase term for the same reason described in the Section3.1.2. However, unlike orbital error estimation in PSI, since the interferometric phases are already unwrapped, we can simply estimate the phase ramp by plane parameters estimating method. All the refined interferograms are then calibrated with respect to the benchmark CI.7-1 where the leveling point shows least variation in time series deformation. As for the remaining process, we simply followed Berardino et al., 2002 other than that we used same filter for residual phase as is described in PSI.

Since displacement values measured from SAR along the radar Line-Of-Sight (LOS) direction, to compare the deformation result with leveling data, the estimated deformation is simply divided by cosine of the incidence angle at the points assuming that there is no significant horizontal displacement in the study area.

3.3 Combination of the results estimated by PSI and SBAS

We subtracted the result of mean deformation velocity by SBAS from the same result by PSI. SBAS result is resampled to the single-look resolution and interpolated so that the subtraction from PSI result can be achieved.

4. RESULTS

First, SBAS-driven deformation time series at Bangkok region is shown in Figure 3. The result was calibrated with respect to one of the leveling stations, CI.7-1. The result showed that the land in the area of Bangkok was deforming at different rates ranging between -23 mm/year (subsiding) and 14 mm/year (uplifting). It can be seen that the city center of Bangkok show relatively small deformation and partly uplifting whereas the outskirt of the region show larger deformation.

Then, we compared the deformation results derived by using SBAS and the field survey data by using GPS. Note that the temporal sampling late of the leveling survey is much lower than the SAR acquisition. In order to quantitatively compare the displacement time series measured from both techniques, spline interpolation was carried out on the SBAS-measurement in the time domain. The SBAS-driven deformation time series corresponding to the leveling stations were interpolated to the beginning of every year from 2008 to 2011. We compared the SBAS-interpolated deformation time series and GPS-driven deformation time series for 14 leveling stations. The differences vary from -42 mm to 7 mm, and the average absolute difference is 6 mm. Finally, the slip-up detection map in a part of the study area around the airport is shown in Figure 4. The values range from -27 mm/year to 31 mm/year for Area A. The mean value and the standard deviation of the result are 2 mm/year and 9 mm/year for Area A, respectively.

We compared DInSAR-driven slip-up velocities with field survey-measured slip-up velocities at 18 sites in Area A. We estimated field survey-driven slip-up velocities from the vertical gaps measured in our field survey, shown in Figure 1, and from the information about the completion of construction year of each building. In case the information about construction year is not available, we assumed the building had been completed 10 years before. In estimating DInSAR-driven slip-up velocities at the sites, we searched 5 nearest points, and calculated mean values. The DInSAR-driven slip-up velocities at 18 sites range from 7 mm/year to 18 mm/year, and that of field survey-driven slip up velocities range from 2 mm/year to 70 mm/year, respectively, and the mean velocities of them are 14 mm/year and 19 mm/year, respectively.

5. DISCUSSION

We compared the results estimated by using SBAS with the annual leveling data, and the reliability of SBAS results was investigated. Overall, two measurements are in a good agreement. The average absolute difference of 6 mm/year is relatively acceptable for L-band DInSAR analysis. The possible reasons of causing the differences between two measurements are as follows; the accuracy of leveling survey, the lack of exact acquisition time of the annual leveling data, poor temporal overlap between datasets, the scale difference of measured targets, and low coherence of the leveling sites.

As for the validation of our slip-up velocity estimation approach, the estimated mean velocity at 18 sites is 14 mm/year whereas the mean velocity of the whole area A is 2 mm/year. We could extract a tendency of slip-up phenomena around the sites. However, as a whole, DInSAR-driven slip-up map underestimated velocities at the sites, compared to field survey ones. Reasons for the difference can be considered as follows. Firstly, for the reason of underestimation may be mainly due to the underestimation of land subsidence by SBAS. Since we currently simply apply multilooking using boxcar window, it is highly possible that the estimated deformation velocities also include that of buildings, leading underestimation of land subsidence (in case the buildings are supported by pile foundation and show no sinking). As a result, DInSAR-driven slip-up velocities can be underestimated. Statistical analysis to exclude such pixels should be taken into account for multilooking process in SBAS in our future work. Similarly, the deformation estimation result of PSI can be also affected by the signal from the land surface. Hence, use of higher resolution SAR images is desirable as well. Secondly, field survey-driven slip-up velocities may be overestimated. Although we assumed the buildings at the sites without the information about construction year had been completed 20 years before for the calculation of the slip-up velocities, those buildings may be built longer ago. As a result, field survey-driven slip-up velocities can be overestimated. Other reasons of the inconsistency of the both measurements may stem form limited and relatively recent observation period of SAR images acquisitions (from about 2008 to 2011) and the decreasing rate of land subsidence for the study area.

Figure 4 shows that the different tendency between the slip-up velocities of airport buildings and runways is clearly observed. The result may indicate that the whole buildings in the airport have been affected by slip-up phenomena. However, further investigation and analysis must be carried out to support the validity and the possibility of the method.

6. CONCLUSION

In this study, the land surface deformation in Bangkok, Thailand estimated by SBAS analysis as well as potential of DInSAR combination approach to detect slip-up phenomena has been presented. As for PSI analysis, we implemented the idea of phase analysis for the PSCs selection and introduced the step to increase the density of the final result. As for the land surface deformation estimation, the comparisons with the leveling have been carried out. The average absolute difference of 6 mm between two measurements at 14 points shows relatively good agreement for L-band SAR analysis. As for the slip-up occurring area detection, we applied our approach to an area that is suffering from slip-up phenomena. However, further investigation and analysis must be carried out to support the validity and the possibility of the method.

7. REFERENCE

Anuphao, A., 2012. InSAR time series analysis for land subsidence monitoring in Bangkok and its vicinity area, Ph.D. thesis, Department of Survey Engineering, Chulalongkorn University, Thailand.

Berardino, P., Fornaro, G., Lanari, R., and Sansosti, E., 2002. A new algorithm for surface deformation monitoring based on small baseline differential SAR interferograms, IEEE Trans. Geosci. Remote Sens., vol. 40, no. 11,pp. 2375-2383.

Colesanti, C., Ferretti, A., Locatelli, R. and Savio, G., 2003. Multi-platform peranent scatterers analysis: first result.

Second GRSS/ISPRS joint workshop on Data Fusion and Remote Sensing over Urban Areas, Berlin, Germany, pp. 52-56.
Ferretti, A., Prati, C., and Rocca, F., 2000. Nonlinear subsidence rate estimation using permanent scatterers in differential SAR interferometry. IEEE Trans. Geosci. Remote Sens., 38(5), pp. 2202–2212.
Ferretti, A., Prati, C., and Rocca, F., 2001. Permanent scatterers in SAR interferometry. IEEE Trans. Geosci. Remote Sens., 39(1), pp. 8–30.
Hooper, A., and Zebker, H., 2007. Persistent scatterer interferometric synthetic aperture radar for crustal deformation analysis, with application to Volcán Alcedo, Galápagos. J. Geophys. Res., 112(B07407), doi: 10.1029/2006JB004763.
Joaquim, J., S., Antonio, M., R., Ramon, F., H., Luisa, B., Antonio, J., G., Jesús, G., and Carlos, S. G., 2010. PS-InSAR processing methodologies in the detection of field surface deformation-Study of the Granada basin (Central Betic Cordilleras, southern Spain) . J. Geodynamics, 49, pp. 181-189
Phien-wej, N., Giao, H. P., and Nutalaya, P. Land subsidence in Bangkok, Thailand, Engineering Geology, vol. 82, no. 4, pp. 187-201, Feb. 2006.
The Royal Thai Survey Department. 2003. International union of geodesy and geophysics -Thailand reported on the geodetic work period 1999-2002, presented at the XXIII general assembly of the international union of geodesy and geophysics.

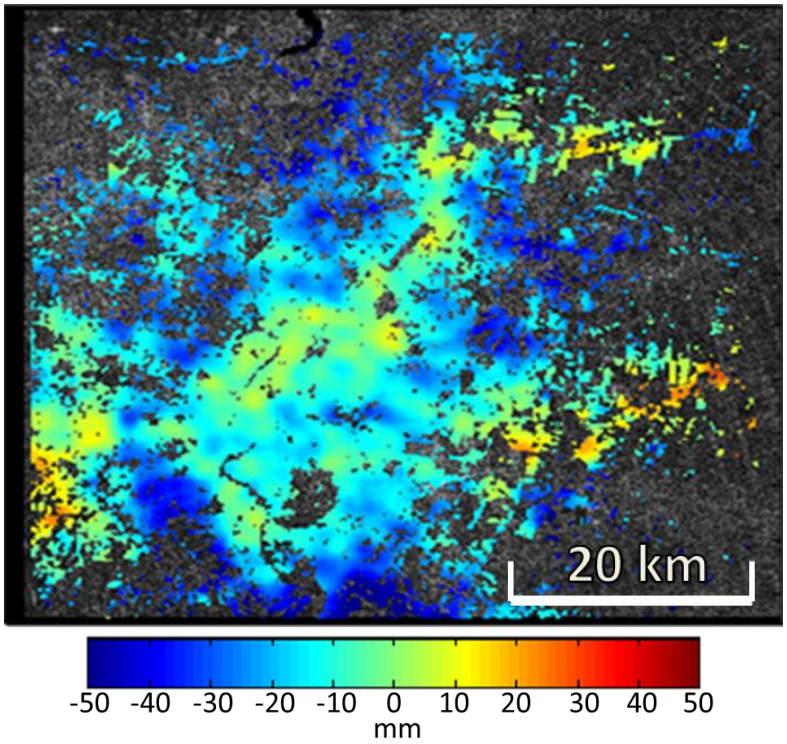

Figure 3. SBAS-driven deformation in Bangkok using ALOS/PALSAR images observed on 25 November 2007 and 3 December 2010.

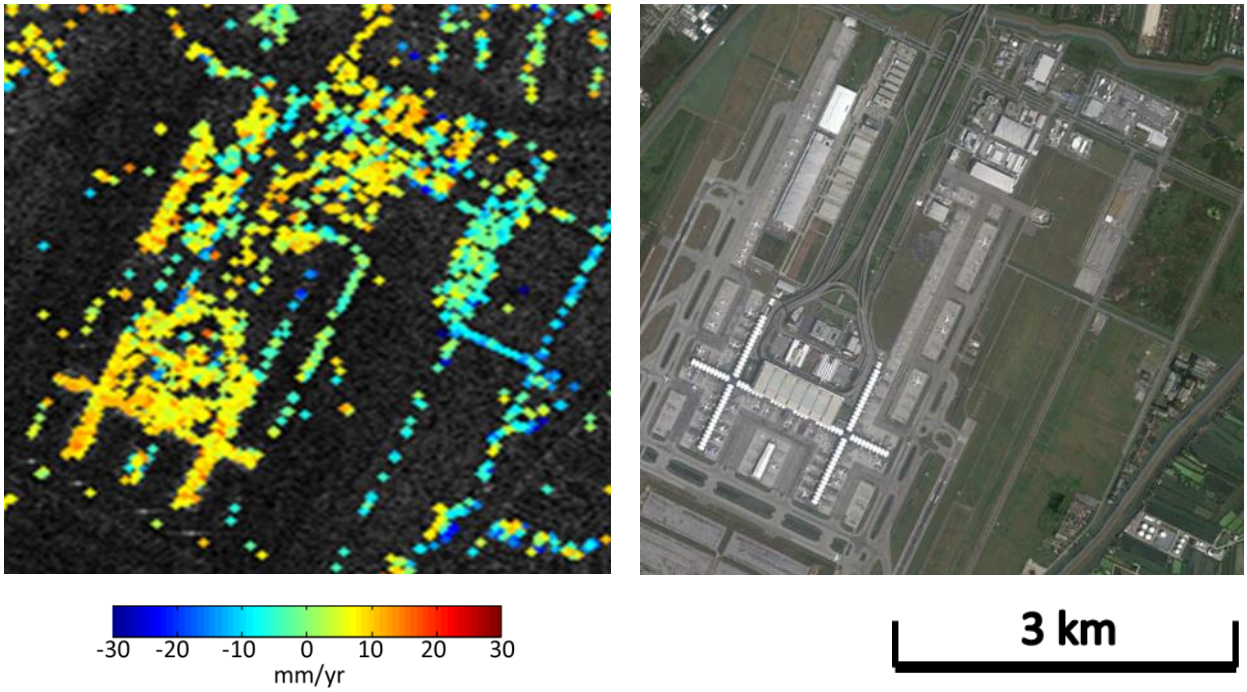

(a) (b)

Figure 4. Slip-up detection map. (a) Slip-up map around Suvarnabhumi Airport in a part of area A. Positive value represents the slip-up occurring area. (b) Google Earth image.